Imaging of polarization-sensitive metasurfaces with quantum entanglement

Charles Altuzarra, Ashley Lyons, Guanghui Yuan, Christy Simpson, Thomas Roger, Jonathan S. Ben-Benjamin, and Daniele Faccio

Phys. Rev. A **99**, 020101 — Published 7 February 2019

DOI: 10.1103/PhysRevA.99.020101

Imaging of polarization sensitive metasurfaces with quantum entanglement

Charles Altuzarra[1,+], Ashley Lyons[2,+], Guanghui Yuan[3,+], Christy Simpson[2], Thomas Roger[4], Jonathan S. Ben-Benjamin[1], Daniele Faccio[2,*]
[1] *Texas A&M University, College Station, Texas 77843-4242, USA*
[2] *School of Physics & Astronomy. University of Glasgow, Glasgow G12 8QQ UK*
[3] *Centre for Disruptive Photonic Technologies, TPI, Nanyang Technological University, 637371, Singapore*
[4] *Institute of Photonics and Quantum Sciences, Heriot-Watt University, EH14 4AS, UK*
(Dated: January 18, 2019)

Quantum entanglement is a key resource that can be exploited for a range of applications such as quantum teleportation, quantum computation and quantum cryptography. However, efforts to exploit entanglement in imaging systems have so far led to solutions such as ghost imaging, that have since found classical implementations. Here we demonstrate an optical imaging protocol that relies uniquely on entanglement: two polarising patterns imprinted and superimposed on a metasurface are separately imaged only when using entangled photons. Un-entangled light is not able to distinguish between the two patterns. Entangled single photon imaging of functional metasurfaces promises advances towards the use of nanostructured subwavelength thin devices in quantum information protocols and a route to efficient quantum state tomography.

Keywords: Plasmonic metasurfaces, Correlated imaging, Quantum imaging, Polarisation measurements

Introduction. Quantum imaging has yielded many advantages including enhancement of spatial resolution beyond the diffraction limit [1, 2], sub-shot-noise imaging [3, 4], ghost imaging [5–9] and the ability to image with photons that are never detected [10]. Of particular interest to this study are imaging techniques whereby an image can only be obtained with one photon when a non-local measurement is performed on another, namely ghost imaging and works concerning the imaging of undetected photons. Both these techniques were originally demonstrated with quantum entangled pairs of photons, and indeed the first impression was that these techniques relied on the unique properties of quantum entanglement and specifically on the nonlocal nature of entanglement that allows for control of a measurement through another measurement performed at different place and time. However, both of these procedures have since been shown to only depend on correlation measurements that are also possible with classical states of light [11–13]. Take, as an example, ghost imaging which is a procedure where an image is formed using a detector that records no spatial information (i.e. a bucket detector) by evaluating the correlations between the bucket detector measurement and a second spatially resolved measurement. Where previously it was thought that this could only be achieved with pairs of photons entangled in the spatial domain, the two photons in fact are only required to share some spatial correlation. Nevertheless, in particular with reference to ghost imaging, these quantum-inspired techniques have lead to a variety of novel imaging methods [14–17].

Metamaterials and their 2-Dimensional counterparts, metasurfaces, have recently started to emerge as a platform that is viable for quantum processing at the single photon level. The first pioneering works demonstrated that quantum entanglement could be preserved in transmission through a metasurface [18], followed by evidence that photon indistinguishability could be preserved in passing from photons to plasmons, thus allowing to perform simple quantum processing steps such as Hong-Ou-Mandel bunching experiments directly on plasmonic chip [19]. Recent experiments have also highlighted how the losses associated with metasurfaces may be harnessed as a resource [20, 21] to thus control the transmitted photon statistics [22–24].

Recent advances in metasurface optical design have provided ultra-thin devices that are capable of controlling and shaping the optical properties of a light beam, for example polarisation, orbital angular momentum (OAM) and focusing. More complex devices are also possible whereby the output depends on the input properties, for example the output OAM or an output holographic image can be controlled by varying the input polarisation [25–27]. These approaches have also very recently been extended to the quantum regime, showing generation and control of entanglement at the metasurface [28, 29].

In the following work we introduce a quantum imaging protocol that fundamentally depends on non-classical photon correlations where images are formed only in the presence of entanglement. We show that single photons transmitted through a polarisation sensitive metasurface with imprinted with two different patterns can produce clear images (either a star or a triangle) only when a corresponding measurement is performed on its polarisation entangled partner photon. Conversely, in cases where entanglement is not present, a composite image is observed (the sum of both the star and triangle) regardless of any post-selection on the photons. Moreover, in gen-

eral, degrading the photon pair entanglement degrades the quality of the image.

Experiment. The experimental setup is shown in Fig. 1. We generated pairs of photons with orthogonal polarisations at a wavelength of 808 nm by Spontaneous Parametric Down-Conversion (SPDC) in a type-II PPKTP nonlinear crystal that was pumped by a continuous-wave 100 mW laser at 404 nm wavelength. The polarisation entangled state is generated using a counter-propagating Sagnac interferometer enclosing the PPKTP crystal [30, 31]. The input 404 nm pump laser beam polarisation is fully controlled by $\lambda/4$ and $\lambda/2$ waveplates and is split into two counterpropagating beams at the polarisation beam-splitter (PBS). Two-wavelength waveplates rotate the polarisation of the pump, without affecting the SPDC photon polarisation (indicated as $\lambda 1$) and of the SPDC photons, without affecting the pump polarisation (indicated as $\lambda 2$). We label photons propagating in the two output modes of the PBS "*herald*" (upwards) and "*signal*" (right). The Sagnac interferometer thus produces an entangled output state from the PBS of the form $|H_h V_s\rangle + |V_h H_s\rangle$ where the subscripts (h, s) denote the herald and signal photons respectively. The herald photon is detected with a Single Photon Avalanche Diode (SPAD), the output of which was connected to the external trigger of an intensified-CCD camera (iCCD, ANDOR iStar) and thus heralds the arrival of a photon at the camera sensor. The second photon of the pair, the signal photon, was optically delayed by 40 m of optical fiber (in order to compensate for the electronic delay acquired by the iCCD camera between the trigger arrival and the actual acquisition on the iCCD sensor) before being focused onto the metasurface sample and imaged onto the iCCD sensor by a pair of $\times 10$ objective lenses (not shown for simplicity in Fig. 1).
In Fig. 2 we show the metasurface that has with two different patterns, a star and a triangle, that also act as polarisers i.e., they only transmit horizontally and vertically polarised light, respectively.

Quantum metasurface theory. In our experiment, we produce photon pairs in two states; a mixed state and a pure state. We produce the mixed state $\hat{\rho}_{\text{mixed}}$

$$\hat{\rho}_{\text{mixed}} = \frac{1}{2}\,|H_h V_s\rangle\langle H_h V_s| + \frac{1}{2}\,|V_h H_s\rangle\langle V_h H_s| \tag{1}$$

where the herald photon, denoted by a subscript 'h', travels to the SPAD, and the signal photon, denoted by a subscript 's', travels to the iCCD. See Fig. 1. with classical probabilities $\frac{1}{2}$ for the two terms, and we produce the pure state $\hat{\rho}_{\text{pure}}$

$$\begin{aligned}\hat{\rho}_{\text{pure}} &= \frac{1}{2}\Big(|H_h V_s\rangle - |V_h H_s\rangle\Big)\Big(\langle H_h V_s| - \langle V_h H_s|\Big)\\ &= \frac{1}{2}\Big(|H_h V_s\rangle\langle H_h V_s| - |H_h V_s\rangle\langle V_h H_s|]\\ &\qquad - |V_h H_s\rangle\langle H_h V_s| + |V_h H_s\rangle\langle V_h H_s|\Big).\end{aligned} \tag{2}$$

where we have the same probability amplitude of the signal and herald photons being in the HV state as vice versa, where H and V stand for the Horizontal and Vertical polarization states of the photon, respectively. In addition, we actually also producestates in which both photons reach the iCCD, and others, where both go to the SPAD; however, our measuring scheme naturally selects the subensemble excluding those, since they do not yield coincidence counts. To model the heralding of a herald photon with a polariser at some angle ϕ, we multiply the density matrix with the polarisation projection operator $\hat{\chi}$ and perform a partial trace over the herald photon

$$\begin{aligned}\hat{\chi}_h(\phi) &= |\phi\rangle\langle\phi|\\ &= \Big(\cos\phi\,|V_h\rangle + \sin\phi\,|H_h\rangle\Big)\Big(\cos\phi\,\langle V_h| + \sin\phi\,\langle H_h|\Big)\\ &= \cos^2\phi\,|V_h\rangle\langle V_h| + \cos\phi\sin\phi\,|V_h\rangle\langle H_h|\\ &\qquad + \cos\phi\sin\phi\,|H_h\rangle\langle V_h| + \sin^2\phi\,|H_h\rangle\langle H_h|.\end{aligned} \tag{3}$$

Heralding a photon. After heralding a photon through a polariser at some angle ϕ, the (un-normalised) state $\hat{\rho}^{(s)}$ of the signal photon impinging on the metasurface becomes (for our two states, $\hat{\rho}_{\text{mixed}}$ and $\hat{\rho}_{\text{pure}}$)

$$\begin{aligned}\hat{\rho}^{(s)}_{\text{mixed}} &= \text{Tr}_h\Big\{\Big(\hat{\chi}_\phi \otimes \hat{1}_s\Big)\,\hat{\rho}_{\text{mixed}}\Big\}\\ &= \frac{1}{2}\cos^2\phi\,|H\rangle\langle H| + \frac{1}{2}\sin^2\phi\,|V\rangle\langle V|\end{aligned} \tag{4}$$

$$\begin{aligned}\hat{\rho}^{(s)}_{\text{pure}} &= \text{Tr}_h\Big\{\Big(\hat{\chi}_\phi \otimes \hat{1}_s\Big)\,\hat{\rho}_{\text{pure}}\Big\}\\ &= \frac{1}{2}\Big(\sin\phi\,|V\rangle - \cos\phi\,|H\rangle\Big)\Big(\sin\phi\,\langle V| - \cos\phi\,\langle H|\Big)\end{aligned} \tag{5}$$

where we omitted the 's' subscripts since at this level, we have no herald photon and we only have a signal photon.
Passage through metasurface. We model the passage through the metasurface oriented along the angle ξ by the operator

$$\hat{M} = \vartheta_{\blacktriangle}(\xi)\hat{\chi}_s(\xi) + \vartheta_{\bigstar}(\xi)\hat{\chi}_s(\xi + 90^\circ) \tag{6}$$

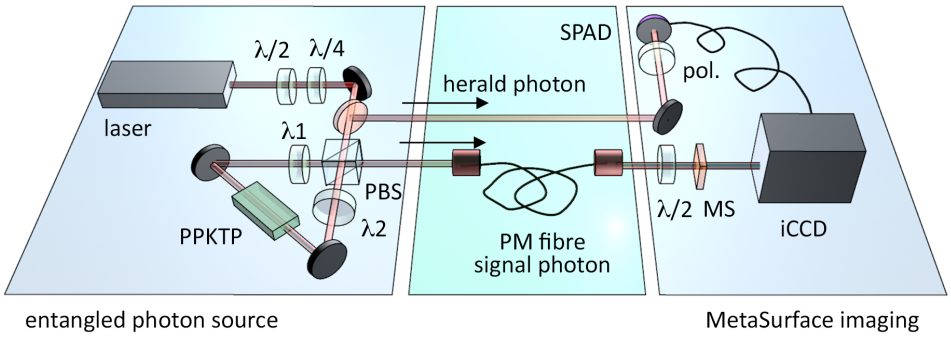

FIG. 1. Polarisation entangled imaging with metasurfaces. Entangled photon pairs are generated within a PPKTP nonlinear crystal surrounded by a Sagnac loop such that it is pumped by two counterpropagating pump beams (controlled by quarter and half-wave plates) from a 404nm CW laser. Two waveplates ($\lambda 1$ and $\lambda 2$) rotate the polarisations of the pump and SPDC photons respectively for one direction around the Sagnac loop. At the polarising beamsplitter (PBS), one photon (the herald) is directed to a polariser (pol.) whilst the other (signal) is transmitted through the polarisation-sensitive plasmonic metasurface (MS) and detected on an iCCD camera. Before the metasurface, we insert an fibre optical delay line so that the photon arrives on the iCCD when the the camera electronic shutter is activated by the herald photon trigger. A half-wave plate placed in front of the metasurface is used to rotate the photon polarisation state by 45° that is equivalent to rotating the metasurface by 45° Light is focused onto the metasurface and then imaged onto the iCCD using microscope objectives (not shown in the figure)

where $\vartheta_{\blacktriangle}(\xi)$ and $\vartheta_{\bigstar}(\xi)$ are the position- and polarisation-dependent transmission amplitude coefficients of the metasurface for the triangle and star respectively when the metasurface is orientated at the angle ξ. See Fig. 2. Considering only the ▲-part (the star part will follow along the same lines), we find that the photon intensity passing through the metasurface is (for our two states, mixed and pure)

$$\begin{aligned} O^{\blacktriangle}_{\text{mixed}} &= \vartheta_{\blacktriangle}(\xi)\text{Tr}\left\{\hat{\chi}_{\xi}\,\hat{\rho}^{(s)}_{\text{mixed}}\right\} \\ &= \frac{1}{2}\vartheta_{\blacktriangle}(\xi)\left[\cos^2\phi\sin^2\xi+\sin^2\phi\cos^2\xi\right] \qquad (7) \\ O^{\blacktriangle}_{\text{pure}} &= \vartheta_{\blacktriangle}(\xi)\text{Tr}\left\{\hat{\chi}_{\xi}\,\hat{\rho}^{(s)}_{\text{pure}}\right\} \\ &= \frac{1}{2}\vartheta_{\blacktriangle}(\xi)\big[\sin^2\xi\cos^2\phi- \\ &\qquad 2\cos\xi\sin\xi\cos\phi\sin\phi+\cos^2\xi\sin^2\phi\big] \qquad (8) \end{aligned}$$

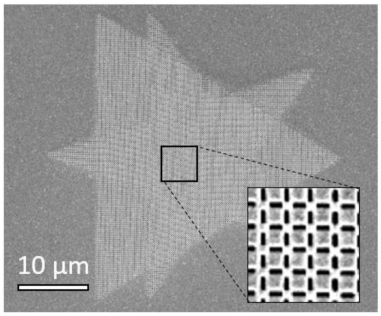

FIG. 2. Metasurface: an image of the metasurface used in the experiments. The two overlaid patterns can be clearly observed: the triangle pattern transmits only horizontally polarised light and the star transmits only vertically polarised light.

The expectation value of the final measurement (i.e., the image that is observed on the iCCD camera) is given by $\langle O\rangle = \text{Tr}(\hat{\rho}\hat{\chi}_h(\phi)\hat{M}(\xi))$, where ϕ is the herald photon polariser angle, which can be nonlocally controlled by the measurement process on the 'herald' arm of the experiment. Similarly, to Eqs. (7) and (8), the intensity of a signal photon transmitted through a pixel in the ★ region of the metasurface is

$$\begin{aligned} O^{\bigstar}_{\text{mixed}} &= \frac{1}{2}\vartheta_{\bigstar}(\xi)\left[\cos^2\phi\cos^2\xi+\sin^2\phi\sin^2\xi\right] \qquad (9) \\ O^{\bigstar}_{\text{pure}} &= \frac{1}{2}\vartheta_{\bigstar}(\xi)\big[\cos^2\phi\cos^2\xi+ \\ &\qquad 2\cos\phi\sin\phi\cos\xi\sin\xi+\sin^2\phi\sin^2\xi\big]. \qquad (10) \end{aligned}$$

To define a visibility, we integrate over the position and normalise the total areas of our signals from both the ★ and ▲ regions. The visibility is

$$V = \frac{O^{\blacktriangle}-O^{\bigstar}}{O^{\blacktriangle}+O^{\bigstar}}, \qquad (11)$$

and using that $O^{\blacktriangle}_{\text{mixed}}+O^{\bigstar}_{\text{mixed}}=1/2$ and that $O^{\blacktriangle}_{\text{pure}}+O^{\bigstar}_{\text{pure}}=1/2$, we find that the visibilities are

$$V_{\text{mixed}} = \left(2\cos^2\phi-1\right)\left(2\sin^2\xi-1\right), \qquad (12)$$

and

$$V_{\text{pure}} = V_{\text{mixed}} - \sin(2\phi)\sin(2\xi). \qquad (13)$$

Eqs. (12) and (13) are confirmed by our experiments. See Fig. 3, where we present the following special cases. Orienting the metasurface at 45°, we find that the visibility

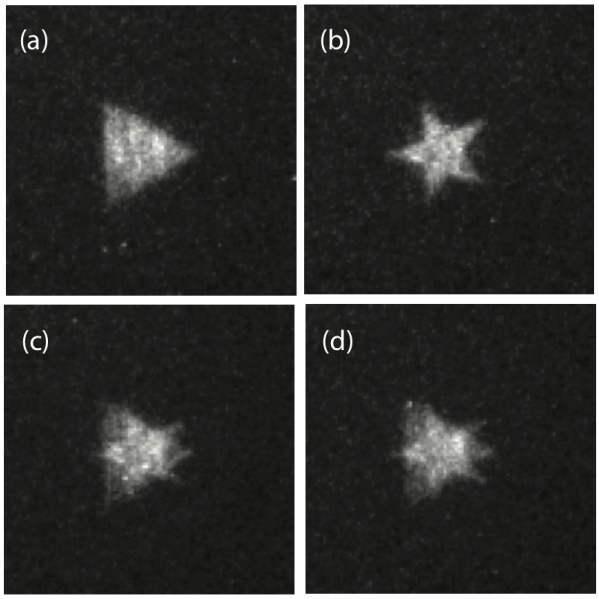

FIG. 3. Imaging with entangled photons: Images obtained with entangled states (measured Bell parameter $S = 2.5$) with the herald polariser selecting photons at (a) 45° and (b) 135° The same images obtained with a mixed state (measured Bell parameter $S = 1.6$) at (c) 45° and (d) 135°

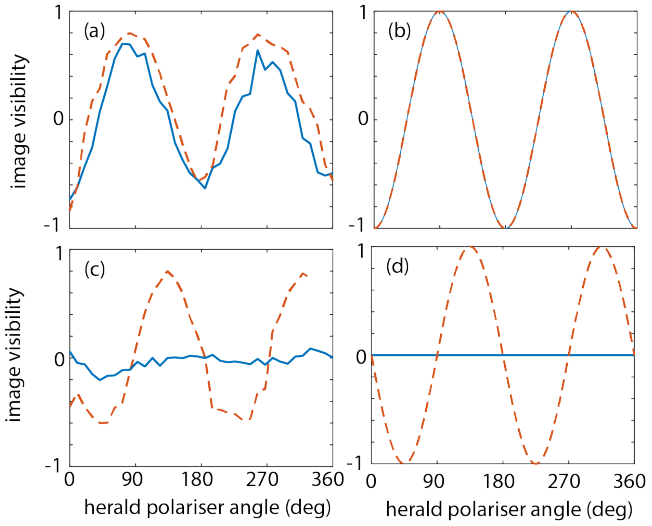

FIG. 4. Imaging with entangled photons: Image visibility, $V = (O_▲ - O_★)/(O_▲ + O_★)$, for the 'triangle' image plotted versus the herald photon polariser angle. Experimental (a) and theoretical (b) results for the case of the metasurface aligned along the H-V axis of the input photons. Experimental (c) and theoretical (d) results for the case of the metasurface aligned at 45° with respect to the polarisation of the input photons. In all figures, solid lines refer to an input mixed state and dashed lines refer to input pure states with measured Bell parameter $S = 2.5$.

of the mixed state is constant (zero), and the visibility of the pure state is $-\sin(2\phi)$. When we orient the metasurface to 0°, we find that both the pure and mixed state visibilities are the same, $-\cos(2\phi)$. Calculation of the expectation value $\langle O \rangle$ reveals that for a mixed (not entangled) state, we will always see a superposition of both the polarisation dependent patterns, i.e. a superposition of a star and a triangle. However, in the presence of a pure quantum state of the form $|\Psi\rangle$, imaging only in the presence of a D (or AD) herald photons will selectively image only the AD (or D) metasurface pattern, i.e. the star or triangle alone will become clearly visible without any overlap of the other.

Figures 3(a) and (b) show the experimental measurements obtained for entangled photons, when selecting D and AD herald photons, respectively. We separately measured the Bell parameter for the photon state used in this experiment to be $S = 2.5$ (i.e. above the threshold $S = 2$ for entanglement and close to the maximally entangled value of $S = 2\sqrt{2}$): the triangle and star are individually very clearly visible, with high contrast and no visible contribution of the other shape. The Sagnac interferometer can also be used to produce a mixed polarisation state by rotating the $\lambda 2$ waveplate to 0° such that the PPKTP crystal is pumped in both directions around the Sagnac loop but there is no compensation for the SPDC-photon temporal walk-off occurring within the crystal.

Entangled state imaging of metasurface structures. Using the experimental layout shown in Fig. 1, we generate an entangled state described by Eq. 2. We place the metasurface in the optical path of the signal photons with a polarisation axis orientated at 45° to the polarisation of the photons. The state has the form

$$\hat{\rho} = \frac{1}{2}\left(|H_h V_s\rangle \langle H_h V_s| + |V_h H_s\rangle \langle V_h H_s| \right) \qquad (14)$$

In this way, the experiment can be repeated with non-entangled photons with a Bell parameter that was measured to be $S = 1.6$. The results are shown in Figs. 3(c) and (d), that look nearly identical regardless of the herald photon polarisation and show a clear superposition of both the star and triangle. Figure 4 shows the full results for these measurements (i.e. for varying angles of the selected herald photon polarisation from 0° to 360° with a direct comparison to the theoretical predictions [32]. In particular, we measure the visibility of the 'triangle' image, $V = (O_▲ - O_★)/(O_▲ + O_★)$. One could use the signal-to-noise-ratio as a possible figure of merit. Here we prefer to use the image visibility at this allows to also make a direct connection to the Bell inequality tests (see below). For the case when the metasurface is aligned with the H-V axis of the input photons ($\xi = 0°$), the theory predicts $V_{\text{pure}} = V_{\text{mixed}} = -\cos(2\phi)$. Alternatively, for the more interesting case in which the metasurface angle $\xi = 45°$, we predict

$$V_{\text{mixed}} = 0, \text{ and } V_{\text{pure}} = -\sin(2\phi) \qquad (15)$$

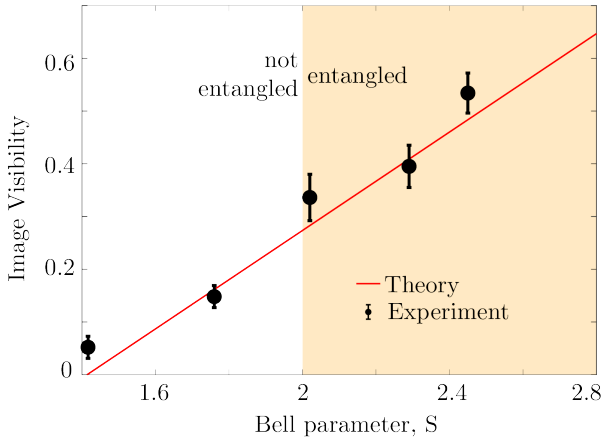

FIG. 5. Imaging with entangled photons: Image visibility for the 'triangle' image plotted versus the herald photon polariser angle for increasing degree of entanglement as measured by the Bell parameter, S. The experimental points show the visibility $V = (O_{\blacktriangle} - O_{\bigstar})/(O_{\blacktriangle} + O_{\bigstar})$ and the theory curve is calculated as $V = (O_{\blacktriangle} - O_{\bigstar})/(O_{\blacktriangle} + O_{\bigstar} + 2\sigma)$ where σ accounts for background noise on the detector that was measured to be 12% of the maximum measured signal.

for the mixed and pure states, respectively. As can be seen in Fig. 4, there is a good agreement between the experiment and theory, although the visibility is lower in the experiment due to background noise on the iCCD sensor. Nevertheless, the main features are clearly observable: Fig.s 4(a) and (b) show the case in which the metasurface is aligned parallel to the H-V polarisation of the photons. The image intensities are essentially identical for the cases of input mixed and pure states, i.e. there is no discernible advantage or difference using entangled states. Conversely, Figs. 4(c) and (d) show the case in which the metasurface is aligned at 45° to the H-V polarisation of the photons: now the un-entangled state shows zero visibility whereas imaging with entangled photons gives rise to clear oscillations in the 'triangle' visibility. Each peak corresponds to all photons being in the 'triangle' image and none in the 'star' image and each trough corresponds to the opposite situation.

In Fig. 5 we show image visibility for the triangle as we gradually increase the degree of entanglement (increasing Bell parameter, S). The experimental points are shown as points with error bars (95% confidence bound of the sinusoidal fits to the curves shown e.g. in Fig. 4). The solid line shows the theoretical prediction based on the model described above accounting also for the detector noise σ that was measured to be of order of 200 counts ($\sim$ 10% of the maximum measured photo counts in the image area), i.e. $V = (O_{\blacktriangle} - O_{\bigstar})/(O_{\blacktriangle} + O_{\bigstar} + 2\sigma)$. The data follow the theoretical expectation and highlight how the image visibility depends the degree of entanglement, dropping to zero for correlated but un-entangled photon pairs and reaching maximum visibility for $S = 2\sqrt{2}$ that is limited only by the noise on the camera.

Conclusions. We have demonstrated an imaging protocol that is inherently dependent on the non-local and superposition properties between a pair of entangled photons. With input states that are entangled and *u*nder the assumption of only H and V photon illumination, it is possible to clearly distinguish the individual images imprinted on the metasurface i.e. individual images become visible only in the presence of pure, entangled states. This functionality is the result of quantum interference occurring on the metasurface, in line with recent reports of 'quantum metamaterials' [28, 29].

The wavelength dependence of metasurfaces may create further opportunities for encrypting sequences of images at different wavelengths for single photon communication channels and the diversity of metasurface designs also opens up the possibility of spatially multiplexed imaging systems which, when combined with time-resolved imaging, can be used for quantum state tomography and exploration of entangled states with imaging techniques. Specifically, this work can be used to build on that demonstrated by Wang et al. [29] whereby a metasurface was designed and fabricated for the purpose of reconstructing the density matrix of a two-photon polarization state. This work required the use of pairs single pixel detectors to perform many two-photon correlation measurements, the number of individual measurements performed could be reduced using the imaging capabilities presented in the work. This becomes particularly advantageous when extending the process to higher dimensional states as discussed in [29].

Acknowledgements. The authors thank Prof. Nikolay Zheludev for fruitful discussions. The authors acknowledge the support of the the support of the Singapore MOE Grants MOE2011-T3-1-005 and MOE2016-T3-1-006, ASTAR QTE Programme Grant SERC A1685b0005, EPSRC (U.K.) grants EP/M009122/1 and EP/J00443X/1 and EU Grant ERC GA 306559. CA acknowledges Robert A. Welch Foundation (Grant No. A-1943-20180324) and the Bio-Photonics initiative of the Texas A&M University. JSB would like to thank the Robert A. Welch Foundation (Grant No. A-1261), Office of Naval Research (Award No. N00014-16-1-3054), and Air Force Office of Scientific Research (FA9550-18-1-0141). for their support.

* + These authors have contributed equally to this work.

Corresponding author: daniele.faccio@glasgow.ac.uk

[1] A. Boto, P. Kok, D. Abrams, S. Braunstein, C. Williams, and J. Dowling, Phys. Rev. Lett. **85**, 2733 (2000), arXiv:9912052 [quant-ph].

[2] M. D'Angelo, M. V. Chekhova, and Y. Shih, Phys. Rev. Lett. **87**, 013602/1 (2001), arXiv:0103035 [quant-ph].

[3] E. Brambilla, L. Caspani, O. Jedrkiewicz, L. A. Lugiato, and A. Gatti, Phys. Rev. A **77**, 053807 (2008).

[4] G. Brida, M. Genovese, and I. R. Berchera, Nat. Photonics **4**, 227 (2010), arXiv:1004.1274.

[5] T. B. Pittman, Y. H. Shih, D. V. Strekalov, and A. V. Sergienko, Phys. Rev. A **52**, R3429 (1995).

[6] D. V. Strekalov, A. V. Sergienko, D. N. Klyshko, and Y. H. Shih, Phys. Rev. Lett. **74**, 3600 (1995).

[7] C. Monken, P. Ribeiro, and S. Pádua, Phys. Rev. A **57**, 3123 (1998).

[8] J. H. Shapiro and R. W. Boyd, Quantum Inf. Process. **11**, 949 (2012).

[9] M. J. Padgett and R. W. Boyd, Philos. Trans. R. Soc. A Math. Phys. Eng. Sci. **375**, 20160233 (2017).

[10] G. B. Lemos, V. Borish, G. D. Cole, S. Ramelow, R. Lapkiewicz, and A. Zeilinger, Nature **512**, 409 (2014).

[11] R. S. Bennink, S. J. Bentley, and R. W. Boyd, Phys. Rev. Lett. **89**, 113601 (2002).

[12] A. Gatti, E. Brambilla, M. Bache, and L. A. Lugiato, Phys. Rev. Lett. **93**, 1 (2004).

[13] J. H. Shapiro, D. Venkatraman, and F. N. C. Wong, Sci. Rep. **5**, 1 (2015).

[14] J. H. Shapiro, Phys. Rev. A **78**, 061802 (2008), arXiv:0807.2614.

[15] B. Sun, M. P. Edgar, R. Bowman, L. E. Vittert, S. Welsh, A. Bowman, and M. J. Padgett, Science **340**, 844 (2013).

[16] A. Kirmani, D. Venkatraman, D. Shin, A. Colaço, F. N. C. Wong, J. H. Shapiro, and V. K. Goyal, Science **343**, 58 (2014).

[17] P. Ryczkowski, M. Barbier, A. T. Friberg, J. M. Dudley, and G. Genty, Nat. Photonics **10**, 167 (2016).

[18] E. Altewischer, M. P. van Exter, and J. P. Woerdman, Nature **418**, 304 (2002).

[19] R. W. Heeres, L. P. Kouwenhoven, and V. Zwiller, Nat. Nanotechnol. **8**, 719 (2013), arXiv:1309.6942.

[20] T. Roger, S. Vezzoli, E. Bolduc, J. Valente, J. J. F. Heitz, J. Jeffers, C. Soci, J. Leach, C. Couteau, N. I. Zheludev, and D. Faccio, Nat. Commun. **6, May**, 7031 (2015).

[21] S. Huang and G. S. Agarwal, Opt. Express **22**, 20936 (2014), arXiv:1402.7146.

[22] C. Altuzarra, S. Vezzoli, J. Valente, W. Gao, C. Soci, D. Faccio, and C. Couteau, ACS Photonics **4**, 2124 (2017).

[23] T. Roger, S. Restuccia, A. Lyons, D. Giovannini, J. Romero, J. Jeffers, M. Padgett, and D. Faccio, Phys. Rev. Lett. **117**, 1 (2016), arXiv:1603.04363.

[24] B. Vest, M. C. Dheur, É. Devaux, A. Baron, E. Rousseau, J. P. Hugonin, J. J. Greffet, G. Messin, and F. Marquier, Science **356**, 1373 (2017).

[25] W. T. Chen, K.-Y. Yang, C.-M. Wang, Y.-W. Huang, G. Sun, I.-D. Chiang, C. Y. Liao, W.-L. Hsu, H. T. Lin, S. Sun, L. Zhou, A. Q. Liu, and D. P. Tsai, Nano Lett. **14**, 225 (2014).

[26] D. Wen, F. Yue, G. Li, G. Zheng, K. Chan, S. Chen, M. Chen, K. F. Li, P. W. H. Wong, K. W. Cheah, E. Yue Bun Pun, S. Zhang, and X. Chen, Nat. Commun. **6**, 1 (2015).

[27] X. Yin, M. Schäferling, B. Metzger, and H. Giessen, Nano Lett. **13**, 6238 (2013).

[28] T. Stav, A. Faerman, E. Maguid, D. Oren, V. Kleiner, E. Hasman, and M. Segev, Science **361**, 1101 (2018).

[29] K. Wang, J. G. Titchener, S. S. Kruk, L. Xu, H.-P. Chung, M. Parry, I. I. Kravchenko, Y.-H. Chen, A. S. Solntsev, Y. S. Kivshar, D. N. Neshev, and A. A. Sukhorukov, Science **361**, 1104 (2018).

[30] T. Kim, M. Fiorentino, and F. N. C. Wong, Phys. Rev. A **73**, 012316 (2006).

[31] A. Fedrizzi, T. Herbst, A. Poppe, T. Jennewein, and A. Zeilinger, Opt. Express **15**, 15377 (2007).

[32] All data is available at DOI: http://dx.doi.org/10.5525/gla.researchdata.704.